

# Effect of Zinc Oxide on the Optical Properties of Polyvinyl Alcohol/Graphene Oxide Nanocomposite

Rania Badry<sup>1</sup> , Maroof A. Hegazy<sup>2</sup>, Ibrahim S. Yahia<sup>3,4,5</sup> , Hanan Elhaes<sup>1</sup> , Heba Y. Zahran<sup>3,4,5</sup>, Medhat A. Ibrahim<sup>6,7,\*</sup> 

<sup>1</sup> Physics Department, Faculty of Women for Arts, Science and Education, Ain Shams University, 11757 Cairo, Egypt; raniabadry806@gmail.com (R.B.); hanan.elhaes@women.asu.edu.eg (H.E.);

<sup>2</sup> National Research Institute of Astronomy and Geophysics (NRIAG), 11421 Helwan, Cairo, Egypt

<sup>3</sup> Research Center for Advanced Materials Science (RCAMS), King Khalid University, Abha 61413, P.O. Box 9004, Saudi Arabia

<sup>4</sup> Laboratory of Nano-Smart Materials for Science and Technology (LNSMST), Department of Physics, Faculty of Science, King Khalid University, P.O. Box 9004, Abha, Saudi Arabia

<sup>5</sup> Nanoscience Laboratory for Environmental and Bio-Medical Applications (NLEBA), Semiconductor Lab., Metallurgical Lab.1., Physics Department, Faculty of Education, Ain Shams University, Roxy, 11757 Cairo, Egypt

<sup>6</sup> Nanotechnology Research Centre (NTRC), The British University in Egypt (BUE), Suez Desert Road, El-Sherouk City, Cairo, 11837, Egypt

<sup>7</sup> Molecular Spectroscopy and Modeling Unit, Spectroscopy Department, National Research Centre, 33 El-Bohouth St., 12622, Dokki, Giza, Egypt

\* Correspondence: Medhat.Ibrahim@bue.edu.eg (M.A.I.);

Scopus Author ID 8641587100

Received: 8.11.2021; Accepted: 5.12.2021; Published: 24.01.2022

**Abstract:** In this work, the conventional casting method was utilized to synthesize nanocomposites based on polyvinyl alcohol (PVA) and both zinc oxide nanoparticles (ZnO-NPs) and graphene oxide (GO). ZnO-NPs have been synthesized by the co-precipitation method while GO with Hummer's method. The synthesized nanocomposites were characterized by UV-vis spectroscopy. Films have been abbreviated to contain different amounts of ZnO as follows: (2, 4, 6, and 8 wt%) and constant amount of GO (2 wt.%) within the PVA matrix using an ultrasonic system to disperse ZnO and GO in the PVA matrix completely. The synthesized nanocomposites were characterized optically by utilizing a UV-Vis-NIR spectrophotometer. The addition of nanofiller to PVA increases the absorption of PVA. At the same time, the optical band gap (for both direct and indirect transitions) was diminished as they depend on the ZnO and GO concentration. PVA/ZnO and PVA/GO nanocomposites present good optical properties. This confirmed that the synthesized ZnO and GO- substituted PAV can be utilized as a solid polymer electrolyte in optoelectronic applications.

**Keywords:** PVA; ZnO nanoparticles; GO and Optical properties.

© 2022 by the authors. This article is an open-access article distributed under the terms and conditions of the Creative Commons Attribution (CC BY) license (<https://creativecommons.org/licenses/by/4.0/>).

## 1. Introduction

Recently, many scientific papers have been published to understand the behavior of polymeric materials. It is especially in its nanocomposite form with nanomaterials such as carbon nanotubes, graphene quantum dots, metals oxides, etc., with some characterizing techniques used to understand the new behavior for this nanocomposite. Due to their trails, optical properties were enhanced [1-4]. Polymer nanocomposites have a wide range of applications due to their unique optical properties as nanomaterials present great promise. This

behavior was confirmed by different spectroscopic techniques such as UV-vis spectrophotometer [5, 6].

Farea M.O. *et al.* (2020) synthesized a polymer blend nanocomposite based on polyethylene oxide and sodium alginate embedded with Au nanoparticles using the casting method and studied their optical and dielectric properties [7]. Meanwhile, Heshmatpour F. *et al.* (2021) synthesized a promising tissue engineering application based on nanocomposites of nanohydroxyapatite and graphene oxide. The prepared nanocomposites were also modified with a natural polymer such as chitosan and synthetic polyethylene glycol [8].

Some applications require certain adjustments to the polymer structure. This reengineering is very troublesome with normal polymers, and thus synthetic polymers, such as polyvinyl alcohol (PVA), polyvinyl chloride (PVC), and polyethylene oxide (PEO), are broadly utilized [9-13]. Polyvinyl alcohol (PVA) is one of the most important synthetic polymers due to its high thermal and mechanical properties [14-16]. The complexation of PVA with other additives occurs due to hydroxyl groups in the PVA structure (i.e., hydrophilic) which facilitate the dispersion process [17]. The hydrophilicity, water-solubility, non-toxicity, biocompatibility of PVA makes it suitable for a wide range of applications, including membranes, drug delivery systems, coatings, adhesives, fuel cells, and electronic devices [18-20].

Pal, N. *et al.* (2021) synthesized a hybrid nanocomposite consisting of cellulose nanocrystal-Ag decorated with reduced graphene oxide sheets through a one-step chemical reduction process [21]. In comparison, Hurayra–Lizu *et al.* (2021) synthesized a nanocomposite material based on Graphene Oxide (GO) and PVA by a facile solution casting method [22]. Thus, the interaction of PVA with different nanofillers such as zinc oxide (ZnO) and graphene oxide (GO) is responsible for such observable improvements due to the presence of oxygenated functional groups. Accordingly, nanocomposites based on PVA substituted with ZnO and GO individually were synthesized using the solution casting method. The importance of these materials was realized when researchers discovered that their size could affect the physicochemical properties of materials, such as their optical properties [23].

Among the different semiconductor materials, ZnO-NPs is a unique electron and wurtzite n-type semiconductor of the broad forward optical band gap of 3.37 eV with high binding energy of 60 meV at ambient temperature [24,25]. The high binding energy of excitons in ZnO will allow it to perform exciton transitions even at ambient temperatures [26]. Because ZnO exhibits similar properties to gallium nitride (GaN) in the short spectral range (green, blue, UV), making it a potential candidate in different optoelectronic devices, biosensors, gas sensors, photocatalysts, and photodetectors [27]. Recently, researchers focused attention on preparing ZnO-NPs to remove organic dyes. Various methods can be utilized to synthesis ZnO-NPs such as sol-gel [28], microwave [29,30], hydrothermal [31], co-precipitation [32], and thermal decomposition methods [33].

On the other hand, oxygenated functional groups in the graphene oxide structure make it easily dispersed in organic solvents, water, and various matrices. This is the main advantage for combining nanostructures with polymeric matrices or ceramic ones to improve their electrical, mechanical, and optical properties [34,35]. Thus, the major purpose of this study is to focus on the good dispersion of ZnO-NPs and GO onto the PVA matrix and study the synthesized nanocomposites optically using UV-Vis spectroscopy.

## 2. Materials and Methods

PVA with a high molecular weight of  $115 \times 10^3$  g/mol was purchased from Export Lab Company, India. Sodium hydroxide ( $\geq 97\%$ ), phosphoric acid (85%), potassium permanganate (99%), and graphite powder were acquired from Fisher Chemical. Meanwhile, sulfuric acid (96%) was acquired from Scharlau and hydrogen peroxide from PIOCHEM (30%). Deionized (DI) Milli-Q water was used during this experiment.

UV-visible spectra of pure PVA, PVA/ZnO, and PVA/GO nanocomposites were collected at room temperature in the 200–800 nm wavelength, using a Jasco V-630 (Japan) spectrophotometer, Spectroscopy Department, National Research Centre, Cairo, Egypt.

The co-precipitation method was utilized to prepare zinc oxide nanoparticles (ZnO-NPs). 1M of zinc acetate dihydrate was dissolved in 100 ml Deionized water at  $70^\circ\text{C}$ . In another Peaker, 2M of sodium hydroxide was dissolved in 100 ml deionized water. Then dropwise sodium hydroxide onto zinc acetate solution with vigorous stirring for 1hr. The white precipitate was separated from the solution by 1000 rpm centrifugation, washing three times using deionized water. The obtained precipitate was dried in a drier overnight at  $80^\circ\text{C}$  and finally calcinated at  $500^\circ\text{C}$  for 2hrs.

Hummer's method was utilized to syntheses GO nanoparticles. In one Peaker,  $\text{H}_2\text{SO}_4$  and  $\text{H}_3\text{PO}_4$  were mixed following the ratio of 9:1. In another Peaker, a mixture of 6 g  $\text{KMnO}_4$  and 1g graphite powder in an ice bath was prepared. Then the two solutions were mixed and stirred for 12hrs at a temperature of  $50^\circ\text{C}$ . After cooling down the mixture (i.e., temperature =  $25^\circ\text{C}$ ), it will be added onto the ice with 1ml of 30%  $\text{H}_2\text{O}_2$ . The precipitate was collected by centrifugation at 10000 rpm, washed the first time with 200ml of 30% HCl, then washed several times with DI water, then dried in a vacuum oven overnight at room temperature.

To dissolve PVA completely, water should be maintained at  $100^\circ\text{C}$  for 30 min before adding PVA powder. Then, 0.5 gm of PVA was dissolved in 50 ml hot aqueous medium under strong stirring for 1 hr until PVA completely dissolved and a white solution was obtained. Next, ZnO-NPs were added to PVA solution with concentrations of 2, 4, 6, and 8 wt% as presented in Table 1. The PVA/ ZnO solution was stirred for additional 2 hrs until ZnO-NPs were dispersed completely within the mixture. The solution was cast in plastic Petri dishes and left to dry in the air for 6 days.

**Table 1.** Composition of PVA nanocomposite films.

Sample	PVA (gm)	ZnO (gm)	GO(gm)
P1	0.50	0.00	0.00
P2	0.49	0.01	0.00
P3	0.48	0.02	0.00
P4	0.47	0.03	0.00
P5	0.46	0.04	0.00
P6	0.49	0.00	0.01

## 3. Results and Discussion

### 3.1. UV-Vis. results.

The UV–Vis. spectra of PVA and PVA/ZnO nanocomposites were recorded in the range of 200-800 nm. The spectra of pristine PVA and that of PVA substituted with different ZnO concentrations (0.01, 0.02, 0.03, and 0.04 g) are shown in Figure 1. The absorption of PVA film increases with increasing the ZnO content in both regions (UV and visible regions), where the PVA spectrum has one absorption band at 278 nm owing to  $\pi\text{-}\pi^*$  transition

corresponding to the C-C vibration. Figure 1 shows that the characteristic band of PVA was shifted to a lower wavelength region due to the addition of ZnO. The intensity of the ZnO characteristic band increases with increasing the ZnO content, and shifts to higher wavelength regions of: 374, 377, 380, and 380 nm for the PVA substituted with 2, 4, 6, and 8 wt% ZnO NPs. This confirms the incorporation of ZnO into the PVA matrix as its position undergoes a redshift and the formation of smaller particle sizes [36,37]. Meanwhile, the UV absorption spectrum of the PVA/GO sample shows an absorption peak at 239 nm, which reflects the  $\pi$ - $\pi^*$  transition.

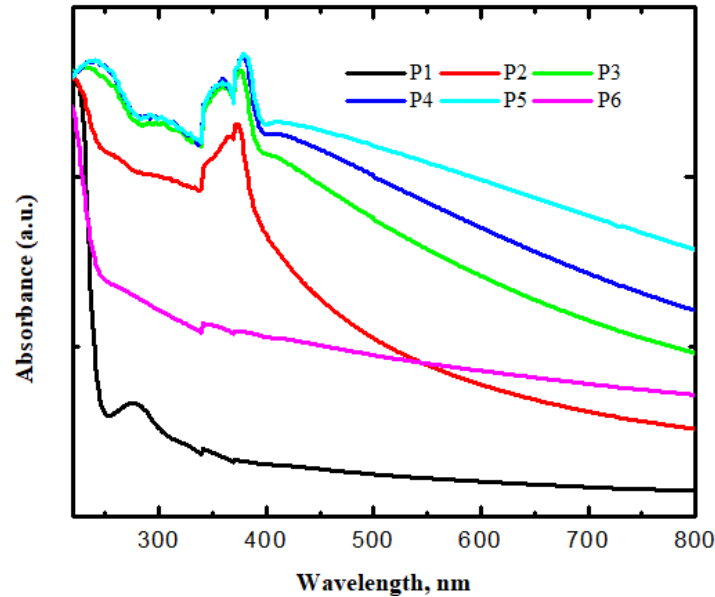


**Figure 1.** UV-Vis absorption spectra of pristine PVA, PVA with 2%, 4%, 6%, 8wt.% of ZnO, and PVA with 2% GO.

### 3.2. Optical absorption coefficient and bandgap energy results.

Equation 1 determines the absorption coefficient ( $\alpha$ ) as a function of wavelength, where A is the absorbance at a specific wavelength and d is the sample thickness.

$$\alpha = (2.303 \cdot A) / d \tag{1}$$

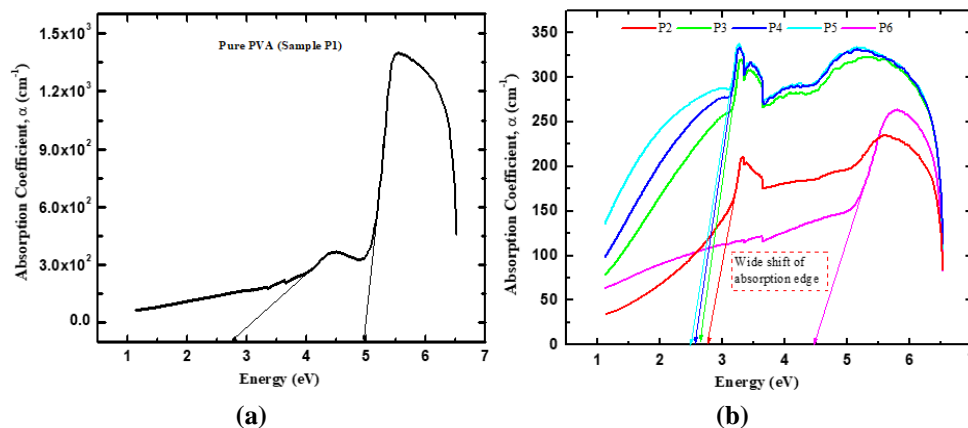


**Figure 2.** The dependence of the absorption coefficient on the photon energy for (a) Pure PVA and (b) PVA/ZnO and GO nanocomposites.

The optical absorption coefficient was determined as a function of the incident photon energy for pure PVA (Figure 2-a) and substituted PVA (PVA/ZnO and PVA/GO), as depicted in Figure 2-b. From the Figure, the absorption edge of pure PVA has been shifted to the lower

energy region with the increase of the ZnO-NPs. However, the difference between the absorption edge of PVA/GO and that of PVA/ZnO is very large. Figure 2- a and b also shows that as the photon energy increases, the absorption coefficient for all samples increases gradually, and then a plateau is observed. Such an increase is linked to the indirect gap semiconductors. The redshift of the absorption edge observed in all samples refers to the bandgap energy decrease. This large shift in the absorption edge may be due to the formation of charge transfer in PVA [38].

Based on Davis and Mott model, the optical bandgap energy can be determined near the edge of fundamental absorption (300-800 nm) using the following equation:

$$(\alpha h\nu)^r = B(h\nu - E_g) \tag{2}$$

where,  $h$  is the plank's constant,  $\nu$  is the frequency,  $r$  is a constant varies according to the transition type,  $B$  is a constant, and  $E_g$  is the optical bandgap [39,40]. Table 2 illustrates the optical band gap values of pure PVA and that of PVA/ZnO nanocomposites. A graph of  $(\alpha h\nu)^2$  versus  $h\nu$  for pure PVA and that treated with ZnO near the absorption edge was presented in Figures 3 and 4, respectively.

**Table 2.** Direct allowed optical band gap energy values for pure PVA and PVA substituted with 2, 4, 6, and 8wt.% ZnO and 2wt.% GO at room temperature.

Sample	Edg <sub>1</sub> (eV)	Edg <sub>2</sub> (eV)	Edg <sub>3</sub> (eV)
P1	3.82	4.93	-
P2	3.11	2.48	4.51
P3	2.96	2.77	3.52
P4	2.94	2.72	3.48
P5	2.92	2.62	3.46
P6	3.17	4.93	-

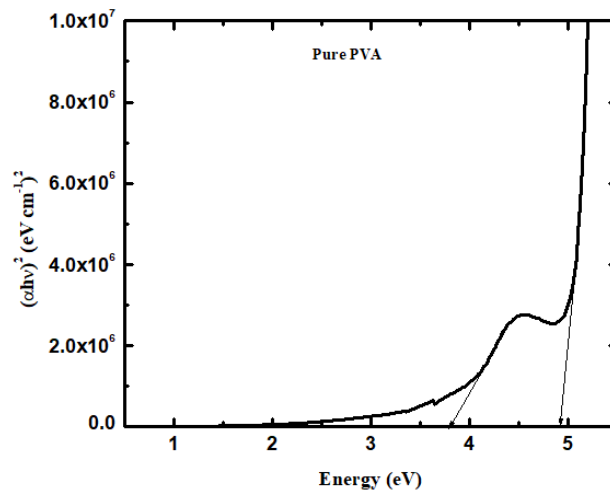


**Figure 3.** The plots of  $(\alpha h\nu)^2$  versus  $h\nu$  for pure PVA.

The linearity in all curves present in Figures 3 and 4 indicates the existence of direct allowed transitions. Extrapolating the linear part to the abscissa gives the corresponding bandwidth  $E_g$ . It is clear from Figure 3 that the linear dependence of pristine PVA appears in two regions, which represent two optical absorption edges as presented in previous work [41]. Films of PVA/ ZnO nanocomposites have three absorption edges and hence three band gaps.

On the other hand, for PVA substituted with GO (sample P6), the variation of  $(\alpha h\nu)^2$  versus photon energy is depicted in Figure 5. The reduction of the PVA optical band gap with

the addition of GO refers to the increase in the defects within the prepared sample of PVA/GO. However, PVA/GO film has only two edges.

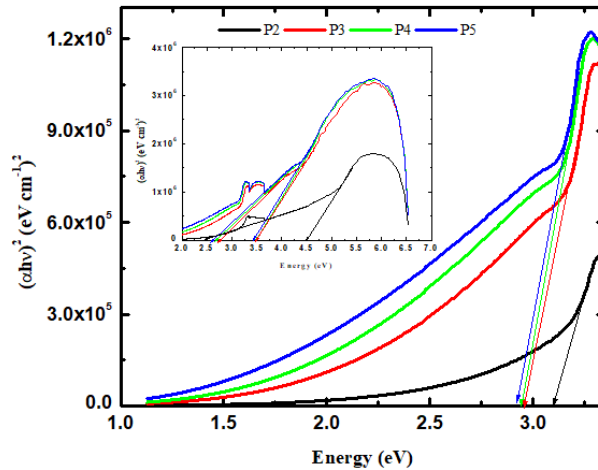


**Figure 4.** The plots of  $(ahv)^2$  versus  $h\nu$  for PVA substituted with 2, 4, 6, and 8wt.% of ZnO with the three absorption shoulders,  $E_{g1}$  together with the inset figure that represents the  $E_{g2}$  and  $E_{g3}$ .

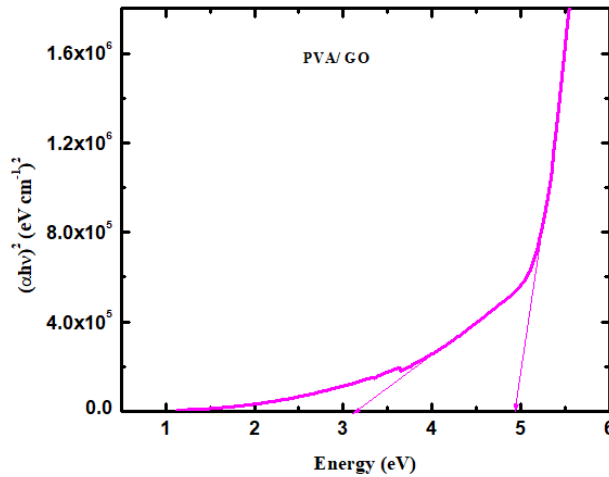


**Figure 5.** The plots of  $(ahv)^2$  versus  $h\nu$  for PVA/GO film.

Each absorption shoulder is characterized by a large optical energy gap,  $E_{g1}$ , and by two smaller ones  $E_{g2}$  and  $E_{g3}$ ; all energy gaps are associated with the electron transitions from the sub energy levels in the valence band to the minimum of the conduction band [42]. The three direct band gaps decrease as the ZnO concentration increases, as shown in Figure 3. Similarly, Table 3 shows the variation in the indirectly allowed energy gaps for pure PVA, PVA/ZnO, and PVA/GO films. The indirectly allowed energy gaps are determined as presented in Figures 6 and 7 for pure PVA and PVA/ZnO and PVA/GO nanocomposites, respectively. The variations in the optical energy gap values present the importance of nanoparticles in modifying the properties of the PVA because of the emergence of defect levels. The localized state's density is proportional to the defect levels concentration and, subsequently, to the ZnO amount. Increasing ZnO content can cause the localized levels to overlap and extend to the gap [43]. This overlap can provide evidence of a decrease in the energy gap as the ZnO concentration increases. The larger optical energy gap is associated with PVA, and its width decreases due to the Zn ions. It is claimed that the smaller absorption shoulders ( $E_{g2}$  and  $E_{g3}$ ) confirm the existence of another state that depends on the ZnO NPs concentration. However,

only one absorption edge was observed in PVA substituted with larger than 2wt.% ZnO and with GO.

**Table 3.** Indirect allowed optical band gap energy values for pure PVA and PVA substituted with 2, 4, 6, and 8wt.% ZnO and that with 2wt.% GO at room temperature.

Sample	Edg <sub>1</sub> (eV)	Edg <sub>2</sub> (eV)
P1	2.60	4.77
P2	2.64	2.90
P3	2.56	-
P4	2.54	-
P5	2.51	-
P6	4.36	-

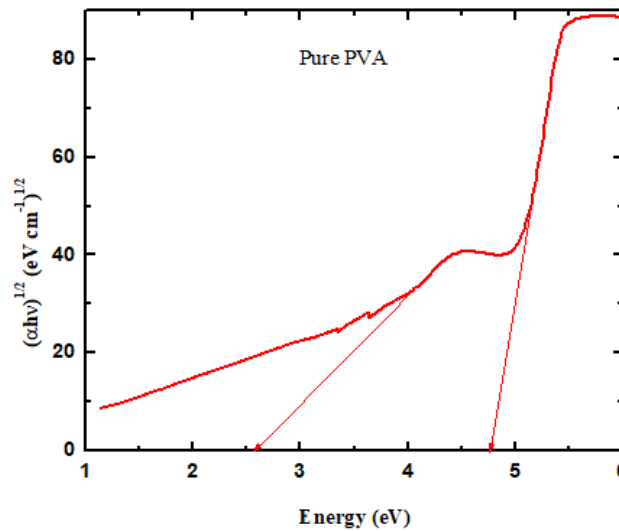


**Figure 6.** The plots of  $(\alpha h\nu)^{1/2}$  versus  $h\nu$  for pure PVA.

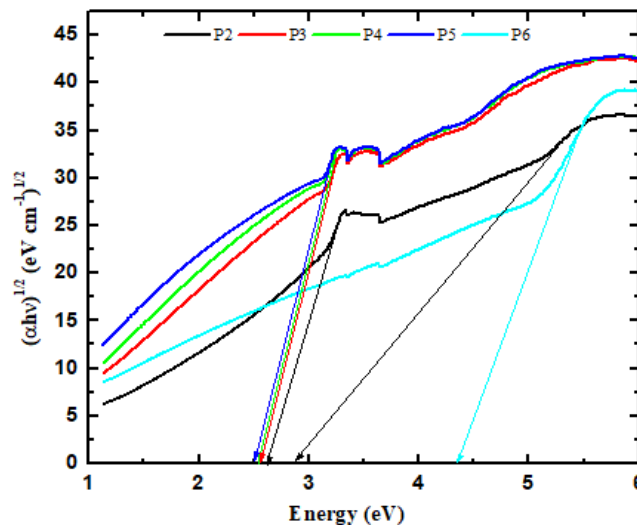


**Figure 7.** The plots of  $(\alpha h\nu)^{1/2}$  versus  $h\nu$  for PVA substituted with 2, 4, 6 and 8wt.% ZnO and that with 2wt.% GO.

#### 4. Conclusions

This work presents the synthesis of PVA nanocomposite (PVA/ZnO and PVA/GO) through the simple solution casting technique. The results showed that the absorption and the absorption coefficient of pure PVA and PVA nanocomposites increase with increasing filler content, which can exhibit a large surface area and good optical properties. Pure PVA possesses an absorption band at 278 nm that reflects the  $\pi$ - $\pi^*$  transition with decreased intensity at higher ZnO content. The results confirmed that pure PVA has two direct absorption edges while

PVA/ZnO has three edges with respect to the electronic transitions between sub levels. Furthermore, the energy gap values decreased with ZnO increases for direct and indirect transitions. This recommended that PVA/ZnO nanocomposite can be used in optoelectronic devices due to their lower bandgap.

## Funding

The authors extend their appreciation to the Scientific Research Deanship at King Khalid University and the Ministry of Education in KSA for funding this research work through the project number IFP-KKU-2020/10.

## Acknowledgments

The authors extend their appreciation to the Deputyship for Research & Innovation, Ministry of Education, in Saudi Arabia, for funding this research work through the project number: (IFP-KKU-2020/10).

## Conflicts of Interest

The authors declare no conflict of interest.

## References

1. Yuan, Z.; Zhao, J.; Meng, F.; Qin, W.; Chen, Y.; Yang, M.; Zhao, Y. Sandwich-like composites of double-layer Co<sub>3</sub>O<sub>4</sub> and reduced graphene oxide and their sensing properties to volatile organic compounds. *Journal of Alloys and Compounds*, **2019**, *793*, 24-30, <https://doi.org/10.1016/j.jallcom.2019.03.386>.
2. Meng, F.; Chang, Y.; Qin, W.; Yuan, Z.; Zhao, J.; Zhang, J.; Ibrahim, M. ZnO-reduced graphene oxide composites sensitized with graphitic carbon nitride nanosheets for ethanol sensing. *ACS Applied Nano Materials*, **2019**, *2*, 2734-2742, <https://doi.org/10.1021/acsanm.9b00257>.
3. Bayoumy, A.M.; Refaat, A.; Yahia, I.S.; Zahran, H.Y.; Elhaes, H.; Ibrahim, M.A.; Shkir, M. Functionalization of graphene quantum dots (GQDs) with chitosan biopolymer for biophysical applications. *Optical and Quantum Electronics*, **2020**, *52*, 1-14, <https://doi.org/10.1007/s11082-019-2134-z>.
4. Bayoumy, A.M.; Ibrahim, M.; Omar, A. Mapping molecular electrostatic potential (MESP) for fulleropyrrolidine and its derivatives. *Optical and Quantum Electronics*, **2020**, *52*, 1-13, <https://doi.org/10.1007/s11082-020-02467-6>.
5. Fu, S.; Sun, Z.; Huang, P.; Li, Y.; Hu, N. Some basic aspects of polymer nanocomposites: A critical review. *Nano Materials Science*, **2019**, *1*, 2-30, <https://doi.org/10.1016/j.nanoms.2019.02.006>.
6. Okasha, A.; Gomaa, F.; Elhaes, H.; Morsy, M.; El-Khodary, S.; Fakhry, A.; Ibrahim, M. Spectroscopic analyses of the photocatalytic behavior of nano titanium dioxide. *Spectrochimica Acta Part A: Molecular and Biomolecular Spectroscopy*, **2015**, *136*, 504-509, <https://doi.org/10.1016/j.saa.2014.09.063>.
7. Farea, M.O.; Abdelghany, A.M.; Oraby, A. H. Optical and dielectric characteristics of polyethylene oxide/sodium alginate-modified gold nanocomposites. *RSC Advances*, **2020**, *10*, 37621-37630, <https://doi.org/10.1039/D0RA07601E>.
8. Heshmatpour, F.; Haghbin, S. Nanohydroxyapatite/graphene oxide nanocomposites modified with synthetic polymers: promising materials for bone tissue engineering applications. *International Journal of Polymeric Materials and Polymeric Biomaterials*, **2021**, *70*, 585-591, <https://doi.org/10.1080/00914037.2020.1740990>.
9. Bharadwaz, A.; Jayasuriya, A. C. Recent trends in the application of widely used natural and synthetic polymer nanocomposites in bone tissue regeneration. *Materials Science and Engineering: C*, **2020**, *110*, 110698, <https://doi.org/10.1016/j.msec.2020.110698>.
10. Xu, H.; Fan, X.; Song, Y.; Zheng, Q. Reinforcement and Payne effect of hydrophobic silica filled natural rubber nanocomposites. *Composites Science and Technology*, **2020**, *187*, 107943, <https://doi.org/10.1016/j.compscitech.2019.107943>.
11. Shakir, M.S.; Khosa, M.K.; Zia, K.M.; Saeed, M.; Bokhari, T.H.; Zia, M.A. Investigation of thermal, antibacterial, antioxidant and antibiofilm properties of PVC/ABS/ZnO nanocomposites for biomedical

- applications. *Korean Journal of Chemical Engineering*, **2021**, 1-6, <https://doi.org/10.1007/s11814-021-0866-5>.
12. Rouabah, N.; Boudine, B.; Nazir, R.; Zaabat, M.; Sebais, M.; Halimi, O.; Chala, A. Structural, optical and photocatalytic properties of PVC/CdS nanocomposites prepared by soft chemistry method. *Journal of Inorganic and Organometallic Polymers and Materials*, **2021**, *31*, 1102-1110, <https://doi.org/10.1007/s10904-020-01752-x>.
  13. Dhatarwal, P.; Sengwa, R.J. Structural, dielectric dispersion and relaxation, and optical properties of multiphase semicrystalline PEO/PMMA/ZnO nanocomposites. *Composite Interfaces*, **2021**, *28*, 827-842, <https://doi.org/10.1080/09276440.2020.1813474>.
  14. Sharifi, F.; Bai, Z.; Montazami, R.; Hashemi, N. Mechanical and physical properties of poly (vinyl alcohol) microfibers fabricated by a microfluidic approach. *RSC advances*, **2016**, *6*, 55343-55353, <https://doi.org/10.1039/C6RA09519D>.
  15. Abdullah, O.G.; Aziz, S.B.; Saber, D.R.; Abdullah, R.M.; Hanna, R.R.; Saeed, S.R. Characterization of polyvinyl alcohol film doped with sodium molybdate as solid polymer electrolytes. *Journal of Materials Science: Materials in Electronics*, **2017**, *28*, 8928-8936, <https://doi.org/10.1007/s10854-017-6623-1>.
  16. Madhuri, S.N.; Murugendrappa, M. V.; Rukmani, K. Conduction and relaxation mechanisms in gadolinium oxide nanoparticle doped polyvinyl alcohol films. *Materials Today Communications*, **2020**, *23*, 100942, <https://doi.org/10.1016/j.mtcomm.2020.100942>.
  17. Kucko, N.W.; de Lacerda Schickert, S.; Sobral Marques, T.; Herber, R.P.; Van den Beuken, J.J.; Zuo, Y.; Leeuwenburgh, S. C. Tough and osteocompatible calcium phosphate cements reinforced with poly (vinyl alcohol) fibers. *ACS Biomaterials Science & Engineering*, **2019**, *5*, 2491-2505, <https://doi.org/10.1021/acsbiomaterials.9b00226>.
  18. Sapalidis, A.A. Porous Polyvinyl alcohol membranes: Preparation methods and applications. *Symmetry*, **2020**, *12*, 960, <https://doi.org/10.3390/sym12060960>.
  19. Yang, J.M.; Fan, C.S.; Wang, N.C.; Chang, Y.H. Evaluation of membrane preparation method on the performance of alkaline polymer electrolyte: Comparison between poly (vinyl alcohol)/chitosan blended membrane and poly (vinyl alcohol)/chitosan electrospun nanofiber composite membranes. *Electrochimica Acta*, **2018**, *266*, 332-340, <https://doi.org/10.1016/j.electacta.2018.02.043>.
  20. Jayakumar, A.; Radoor, S.; Nair, I.C.; Siengchin, S.; Parameswaranpillai, J.; Radhakrishnan, E.K. Lipopeptide and zinc oxide nanoparticles blended polyvinyl alcohol-based nanocomposite films as antimicrobial coating for biomedical applications. *Process Biochemistry*, **2021**, *102*, 220-228, <https://doi.org/10.1016/j.procbio.2020.12.010>.
  21. Pal, N.; Banerjee, S.; Roy, P.; Pal, K. Cellulose nanocrystals-silver nanoparticles-reduced graphene oxide based hybrid PVA nanocomposites and its antimicrobial properties. *International Journal of Biological Macromolecules*, **2021**, *191*, 445-456. <https://doi.org/10.1016/j.ijbiomac.2021.08.237>
  22. Hurayra-Lizu, K.A.; Bari, M.W.; Gulshan, F.; Islam, M.R. GO based PVA nanocomposites: tailoring of optical and structural properties of PVA with low percentage of GO nanofillers. *Heliyon*, **2021**, *7*, e06983, <https://doi.org/10.1016/j.heliyon.2021.e06983>.
  23. Khan, I.; Saeed, K.; Khan, I. Nanoparticles: Properties, applications and toxicities. *Arabian journal of chemistry*, **2019**, *12*, 908-931, <https://doi.org/10.1016/j.arabjc.2017.05.011>.
  24. Oktaviani, O. Nanoparticles: Properties, applications and toxicities. *Jurnal Latihan*, **2021**, *1*, 11-20. <https://doi.org/10.1016/j.arabjc.2017.05.011>.
  25. Talam, S.; Karumuri, S.R.; Gunnam, N. Synthesis, characterization, and spectroscopic properties of ZnO nanoparticles. *International Scholarly Research Notices*, **2012**, *2012*, <https://doi.org/10.5402/2012/372505>.
  26. Widiyandari, H.; Umiati, N.A.K.; Herdianti, R.D. Synthesis and photocatalytic property of Zinc Oxide (ZnO) fine particle using flame spray pyrolysis method. In *Journal of Physics: Conference Series*, **2018**, *1025*, 012004, <https://doi.org/10.1088/1742-6596/1025/1/012004>.
  27. Ong, C.B.; Ng, L.Y.; Mohammad, A.W. A review of ZnO nanoparticles as solar photocatalysts: Synthesis, mechanisms and applications. *Renewable and Sustainable Energy Reviews*, **2018**, *81*, 536-551, <https://doi.org/10.1016/j.rser.2017.08.020>.
  28. Hasnidawani, J. N.; Azlina, H. N.; Norita, H.; Bonnia, N. N.; Ratim, S.; Ali, E. S. Synthesis of ZnO nanostructures using sol-gel method. *Procedia Chemistry*, **2016**, *19*, 211-216, <https://doi.org/10.1016/j.proche.2016.03.095>.

29. Sharma, D.; Sharma, S.; Kaith, B. S.; Rajput, J.; Kaur, M. Synthesis of ZnO nanoparticles using surfactant free in-air and microwave method. *Applied Surface Science*, **2011**, *257*, 9661-9672., <https://doi.org/10.1016/j.apsusc.2011.06.094>.
30. Yathisha, R.O.; Nayaka, Y.A.; Vidyasagar, C.C. Microwave combustion synthesis of hexagonal prism shaped ZnO nanoparticles and effect of Cr on structural, optical and electrical properties of ZnO nanoparticles. *Materials Chemistry and Physics*, **2016**, *181*, 167-175, <https://doi.org/10.1016/j.matchemphys.2016.06.046>.
31. Kumaresan, N.; Ramamurthi, K.; Babu, R.R.; Sethuraman, K.; Babu, S.M. Hydrothermally grown ZnO nanoparticles for effective photocatalytic activity. *Applied Surface Science*, **2017**, *418*, 138-146, <http://dx.doi.org/10.1016/j.apsusc.2016.12.231>.
32. Kahouli, M.; Barhoumi, A.; Bouzid, A.; Al-Hajry, A.; Guerhazi, S. Structural and optical properties of ZnO nanoparticles prepared by direct precipitation method. *Superlattices and Microstructures*, **2015**, *85*, 7-23, <https://doi.org/10.1016/j.spmi.2015.05.007>.
33. Nagaraju, G.; Nagabhushana, H.; Basavaraj, R.B.; Raghu, G.K.; Suresh, D.; Rajanaika, H.; Sharma, S.C. Green, nonchemical route for the synthesis of ZnO superstructures, evaluation of its applications toward photocatalysis, photoluminescence, and biosensing. *Crystal Growth & Design*, **2016**, *16*, 6828-6840, <https://doi.org/10.1021/acs.cgd.6b00936>.
34. Sharma, N.; Sharma, V.; Jain, Y.; Kumari, M.; Gupta, R.; Sharma, S.K.; Sachdev, K. Synthesis and characterization of graphene oxide (GO) and reduced graphene oxide (rGO) for gas sensing application. In *Macromolecular Symposia*, **2017**, *376*, 1700006, <https://doi.org/10.1002/masy.201700006>.
35. Fu, S.; Sun, Z.; Huang, P.; Li, Y.; Hu, N. Some basic aspects of polymer nanocomposites: A critical review. *Nano Materials Science*, **2019**, *1*, 2-30, <https://doi.org/10.1016/j.nanoms.2019.02.006>.
36. Menazea, A.A.; Ezzat, H.A.; Omara, W.; Basyouni, O.H.; Ibrahim, S.A.; Mohamed, A.A.; Ibrahim, M.A. Chitosan/graphene oxide composite as an effective removal of Ni, Cu, As, Cd and Pb from wastewater. *Computational and Theoretical Chemistry*, **2020**, *1189*, 112980, <https://doi.org/10.1016/j.comptc.2020.112980>.
37. Moez, A.A.; Ibrahim, M.A.; Gad, S.A. Influence of Annealing Temperatures on Nonlinear Optical, Dielectric, Semiconducting Results, and Fermi Level Position for CdPO. 03Te0. 97 Thin Film. *Bio interface research in applied chemistry*, **2021**, *12*, 1916-1926, <https://doi.org/10.33263/BRIAC122.19161926>.
38. Elashmawi, I.S.; Menazea, A.A. Different time's Nd: YAG laser-irradiated PVA/Ag nanocomposites: structural, optical, and electrical characterization. *Journal of Materials Research and Technology*, **2019**, *8*, 1944-1951. <https://doi.org/10.1016/j.jmrt.2019.01.011>.
39. Aziz, S. B.; Rasheed, M. A.; Ahmed, H. M. Synthesis of polymer nanocomposites based on [methyl cellulose]  $(1-x):(\text{CuS})_x$  ( $0.02 \leq x \leq 0.08$ ) with desired optical band gaps. *Polymers*, **2017**, *9*, 194, <https://doi.org/10.3390/polym9060194>.
40. Badry, R.; Ezzat, H.A.; El-Khodary, S.; Morsy, M.; Elhaes, H.; Nada, N.; Ibrahim, M. Spectroscopic and thermal analyses for the effect of acetic acid on the plasticized sodium carboxymethyl cellulose. *Journal of Molecular Structure*, **2021**, *1224*, 129013, <https://doi.org/10.1016/j.molstruc.2020.129013>.
41. Badry, R.; El-Khodary, S.; Elhaes, H.; Nada, N.; Ibrahim, M. Optical, conductivity and dielectric properties of plasticized solid polymer electrolytes based on blends of sodium carboxymethyl cellulose and polyethylene oxide. *Optical and Quantum Electronics*, **2021**, *53*, 1-15, <https://doi.org/10.1007/s11082-020-02649-2>.
42. Elkomy, G.M.; Mousa, S.M.; Mostafa, H.A. Structural and optical properties of pure PVA/PPY and cobalt chloride doped PVA/PPY films. *Arabian Journal of Chemistry*, **2016**, *9*, S1786-S1792, <https://doi.org/10.1016/j.arabjc.2012.04.037>.
43. Murri, R.; Schiavulli, L.; Pinto, N.; Ligonzo, T. Urbach tail in amorphous gallium arsenide films. *Journal of non-crystalline solids*, **1992**, *139*, 60-66, [https://doi.org/10.1016/S0022-3093\(05\)80805-1](https://doi.org/10.1016/S0022-3093(05)80805-1).